energies

MDPI

Article

Wet Chemical Oxidation to Improve Interfacial Properties of Al_2O_3/Si and Interface Analysis of Al_2O_3/SiO_x/Si Structure Using Surface Carrier Lifetime Simulation and Capacitance–Voltage Measurement

Kwan Hong Min [1,2], Sungjin Choi [1,3], Myeong Sang Jeong [1,2], Sungeun Park [1], Min Gu Kang [1], Jeong In Lee [1], Yoonmook Kang [3], Donghwan Kim [2], Hae-Seok Lee [3,*] and Hee-eun Song [1,*]

[1] Photovoltaics Laboratory, Korea Institute of Energy Research, Daejeon 34129, Korea; steel1217@kier.re.kr (K.H.M.); agape383177@gmail.com (S.C.); jmsang@kier.re.kr (M.S.J.); separk@kier.re.kr (S.P.); mgkang@kier.re.kr (M.G.K.); jilee@kier.re.kr (J.I.L.)

[2] Department of Materials Science and Engineering, Korea University, Seoul 02841, Korea; donghwan@korea.ac.kr

[3] Department of Energy Environment Policy and Technology, Green School (Graduate School of Korea Energy and Environment), Korea University, Seoul 02841, Korea; ddang@korea.ac.kr

* Correspondence: lhseok@korea.ac.kr (H.-S.L.); hsong@kier.re.kr (H.-e.S.)

Received: 6 March 2020; Accepted: 7 April 2020; Published: 8 April 2020

Abstract: A thin silicon oxide (SiO_x) layer (thickness: 1.5–2.0 nm) formed at an Al_2O_3/Si interface can enhance the interface properties. However, it is challenging to control the characteristics of thin SiO_x layers because SiO_x forms naturally during Al_2O_3 deposition on Si substrates. In this study, a ~1.5 nm-thick SiO_x layer was inserted between Al_2O_3 and Si substrates by wet chemical oxidation to improve the passivation properties. The acidic solutions used for wet chemical oxidation were $HCl:H_2O_2:H_2O$, $H_2SO_4:H_2O_2:H_2O$, and HNO_3. The thicknesses of SiO_x layers formed in the acidic solutions were ~1.48, ~1.32, and ~1.50 nm for $SiO_{x\text{-}HCl}$, $SiO_{x\text{-}H2SO4}$, and $SiO_{x\text{-}HNO3}$, respectively. The leakage current characteristics of $SiO_{x\text{-}HNO3}$ were better than those of the oxide layers formed in the other acidic solutions. After depositing a ~10 nm-thick Al_2O_3 on an $SiO_{x\text{-}acidic}$/Si structure, we measured the effective carrier lifetime using quasi steady-state photoconductance and examined the interfacial properties of $Al_2O_3/SiO_{x\text{-}acidic}$/Si using surface carrier lifetime simulation and capacitance–voltage measurement. The effective carrier lifetime of $Al_2O_3/SiO_{x\text{-}HNO3}$/Si was relatively high (~400 µs), resulting from the low surface defect density ($2.35–2.88 \times 10^{10}$ $cm^{-2}eV^{-1}$). The oxide layer inserted between Al_2O_3 and Si substrates by wet chemical oxidation helped improve the Al_2O_3/Si interface properties.

Keywords: aluminum oxide; silicon oxide; quasi steady-state photoconductance; surface passivation; crystalline silicon (c-Si) solar cell; plasma-assisted atomic layer deposition

1. Introduction

The surface passivation of crystalline silicon (c-Si) solar cells can be improved using various materials such as SiO_2 [1–6], SiN_x [7–9], Al_2O_3 [10–13], TiO_x [14–16], MoO_x [17,18], and poly-Si [19–22]. In particular, Al_2O_3 thin films are most widely used for boron-doped Si surfaces (or p^+ emitter surfaces) owing to the low surface recombination velocity (SRV) [10,11]. The interface of Al_2O_3 films can be characterized by a low interface trap density and a high negative charge density because of the ultrathin SiO_x and negatively charged interstitial O ions present at the Al_2O_3/Si interface [23,24]. The passivation

properties of an Al_2O_3/Si structure can be improved by optimizing the Al_2O_3 thickness and annealing temperature [25,26]. In particular, a thin SiO_x layer is formed at the Al_2O_3/Si interface during the deposition process and can be activated through annealing. However, it is difficult to control the quality of this layer because it forms spontaneously.

In this work, we considered a method to improve the interfacial properties of an Al_2O_3/Si structure by inserting a thin silicon oxide layer between Al_2O_3 and Si substrates. The widely used methods of growing thin silicon oxides are thermal and wet chemical oxidations. In thermal oxidation, although the quality of the silicon oxide formed is excellent, it is difficult to control the thickness (<1.5 nm) at temperatures above 800 °C. If the silicon oxide layer becomes thicker, the field effect passivation of the Al_2O_3/Si interface may deteriorate [27]. Therefore, a thickness of ~1.5 nm or less is required to improve the interfacial properties of the Al_2O_3/Si structure and ensure a good field effect passivation. Wet chemical oxidation is a promising method of growing thin SiO_x, and the quality of thin oxides grown using this method has been verified [28–32]. In this research, a thin oxide layer was utilized to improve the passivation property of an Al_2O_3/Si structure. We applied wet chemical oxidation to grow ~1.5 nm-thick SiO_x and then deposited a ~10 nm-thick Al_2O_3 using plasma-assisted atomic layer deposition (PA-ALD). To analyze the passivation characteristics and interface properties of the Al_2O_3/SiO_x/Si structure, the effective carrier lifetime was measured using quasi steady state photoconductance (QSSPC), and surface carrier lifetime simulation and capacitance–voltage (C–V) measurements were performed.

2. Experimental

After the Radio Corporation of America (RCA) cleaning developed by Werner Kern to remove ionic and organic impurities in the polished 4~5 Ω·cm p-type Si(100) substrate [33], we performed wet chemical oxidation using three acidic solutions: (i) $HCl:H_2O_2:H_2O$ = 1:1:5, (ii) $H_2SO_4:H_2O_2:H_2O$ = 1:1:5, and (iii) HNO_3 (68%) [28–30]. The wet chemical oxide layers formed in the acidic solutions are hereinafter abbreviated as $SiO_{x\text{-}HCl}$, $SiO_{x\text{-}H2SO4}$, and $SiO_{x\text{-}HNO3}$, respectively. The process temperature was 85 °C for $SiO_{x\text{-}HCl}$ and $SiO_{x\text{-}H2SO4}$ and 121 °C for $SiO_{x\text{-}HNO3}$. The immersion time was varied from 10 to 60 min. The thickness and refractive index of the silicon oxide ($SiO_{x\text{-}acidic}$) layers formed on Si surface was measured using spectroscopy ellipsometry (SE) and transmission electron microscopy (TEM). The quality of $SiO_{x\text{-}acidic}$ was evaluated in terms of the leakage current density, which was measured by conducting a current–voltage (I–V) analysis with mercury probe and Keithley 238 current source meter under dark conditions. To measure the surface passivation characteristics, an approximately 10 nm-thick Al_2O_3 film was deposited on a $SiO_{x\text{-}acidic}$/Si substrate using PA-ALD. The reaction sources for Al_2O_3 deposition were trimethylaluminum ($Al(CH_3)_3$, TMA) and O_2 (purity 99.999%) gas; the purge gas was Ar (purity 99.999%). The deposition process was performed at a substrate temperature of 250 °C, a process pressure of 1.0 torr, a plasma power of 200 W, an O_2 exposure time of 0.5 s, and a distance of 20 mm between the showerhead and the substrate. Annealing was then conducted in an electric furnace at 425 °C for 15 min to activate the Al_2O_3 layer. After annealing, the carrier lifetimes of the samples were measured using QSSPC to evaluate the surface passivation characteristics. For a detailed analysis of the interface properties of Al_2O_3/$SiO_{x\text{-}acidic}$/Si, a surface carrier lifetime simulation and C–V measurement were performed by mercury probe with Agilent E4980A LCR meter.

3. Results and Discussions

Figure 1 shows the thickness of the silicon oxide ($SiO_{x\text{-}acidic}$) formed in the acidic solutions with various immersion times. The film thickness was measured by SE. The measured wavelength range was 300–100 nm and the incident beam angle was 75° in the SE measurement. With the increase in the immersion time, the thickness increased, saturating in the range of 1.32–1.50 nm. The thicknesses of SiO_x are ~1.48 nm for $SiO_{x\text{-}HCl}$, ~1.32 nm for $SiO_{x\text{-}H2SO4}$, and ~1.50 nm for $SiO_{x\text{-}HNO3}$. These results are similar to those reported previously [28–30]. The thickness of $SiO_{x\text{-}HNO3}$ was also confirmed by TEM

measurement, as shown in Figure 2. In the TEM measurements, silicon nitride (SiN_x) was used as the capping layer to avoid additional thin oxide growth in the Al_2O_3 deposition process. The $SiO_{x\text{-}HNO3}$ thickness was in the range of 1.43–1.54 nm, consistent with SE measurements. As the thicknesses of SiO_x formed in each acidic solution saturated after approximately 15 min, the immersion time was fixed at 15 min (Table 1). To evaluate the characteristics of the $SiO_{x\text{-}acidic}$ layer, the leakage current densities were measured by I–V curves under dark conditions. As shown in Figure 3, the leakage current density of $SiO_{x\text{-}HNO3}$ was the lowest (~9.1×10^{-3} A/cm^2 at 1 $V_{forward\text{-}bias}$ and ~0.92×10^{-3} A/cm^2 at −1 $V_{reverse\text{-}bias}$), indicating that the quality of $SiO_{x\text{-}HNO3}$ is relatively better than the other oxides. The leakage current density results are similar to those reported by Kobayashi Asuha et al. [30].

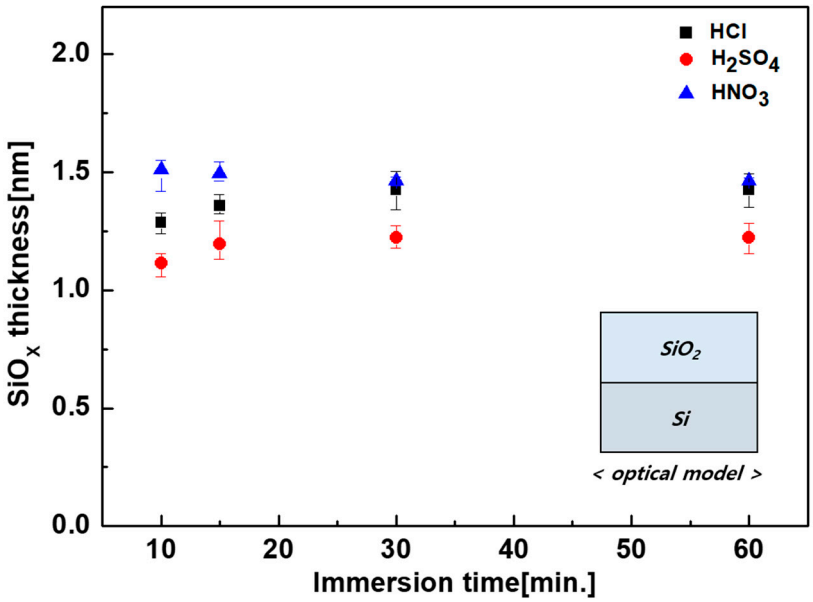

Figure 1. Measured thicknesses of wet chemical oxide (SiO_x) layers prepared in different acid solutions as a function of the immersion time. The optical model is shown in the insert (right bottom) for ellipsometry analysis.

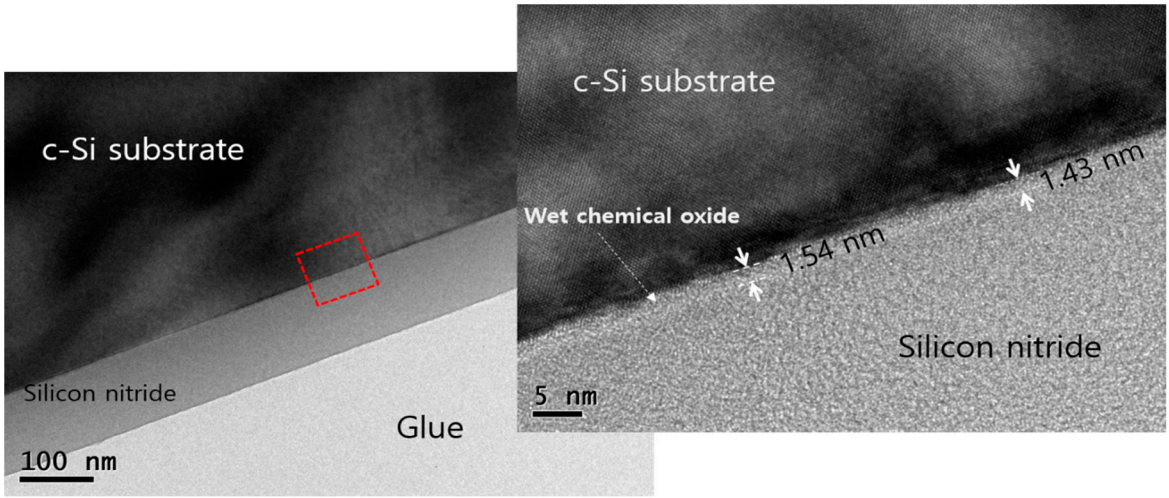

Figure 2. Transmission electron microscopy (TEM) images of the wet chemical oxide ($SiO_{x\text{-}HNO3}$) layer in an $SiN_x/SiO_x/Si$ structure.

Table 1. SiO_x layer thickness and refractive index (n) at an immersion time of 15 min. The data are averaged with ten samples.

Solution	Thickness (nm)	Refractive Index (n) at 630 nm
HCl	1.49	1.421
H_2SO_4	1.32	1.417
HNO_3	1.50	1.430

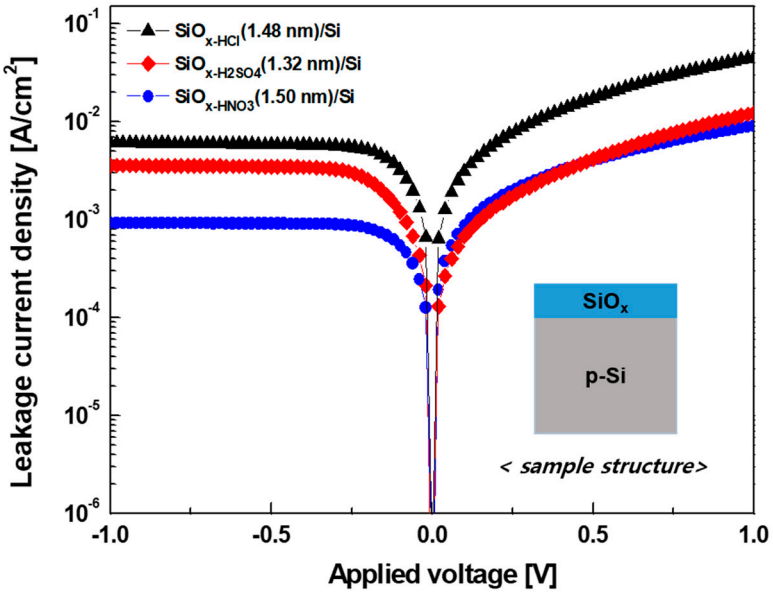

Figure 3. Current–voltage curves under dark condition for SiO_x/Si formed in different acidic solutions. The SiO_x thickness is 1.49 nm for $SiO_{x\text{-}HCl}$, 1.32 nm for $SiO_{x\text{-}H2SO4}$, and 1.50 nm for $SiO_{x\text{-}HNO3}$, respectively.

To investigate the surface passivation properties of the $SiO_{x\text{-}acidic}$, a ~10 nm-thick Al_2O_3 layer was deposited on both sides of the $SiO_{x\text{-}acidic}$/Si substrate using PA-ALD, and the effective carrier lifetime was measured by QSSPC. The measured effective carrier lifetimes at 1.0 sun injection level [34] of $Al_2O_3/SiO_{x\text{-}HNO3}$/Si, $Al_2O_3/SiO_{x\text{-}HCl}$/Si, and $Al_2O_3/SiO_{x\text{-}H2SO4}$ /Si are ~400, ~317, and ~332 μs (Figure 4); notably, the passivation quality of $SiO_{x,HNO3}$ is excellent. Moreover, the reference sample, which did not form an oxide film intentionally, exhibited a significantly lower effective carrier lifetime (~220 μs) than the samples with wet chemical oxides. This indicates that the quality of the thin SiO_x layer formed at the Al_2O_3/Si interface influences the effective carrier lifetime and that the oxides formed in acidic solutions exhibit better passivation properties than oxide films formed naturally during the deposition process. To investigate the interfacial properties of $Al_2O_3/SiO_{x\text{-}acidic}$/Si, the surface carrier lifetime simulation and C–V measurement were performed. The surface carrier lifetime simulation is based on the extended Shockley–Read–Hall (SRH) recombination equation. This equation was derived from the SRV, expressed in Equations (1) and (2) [35,36].

$$S \equiv \frac{U_s}{\Delta n_s} \tag{1}$$

$$U_s = \frac{n_s p_s - n_i^2}{\frac{n_s + n_1}{S_{p0}} + \frac{p_s + p_1}{S_{n0}}} \text{ with } S_{p0} = \sigma_p V_{th} D_{it},\ S_{n0} = \sigma_n V_{th} D_{it} \tag{2}$$

where S is the surface recombination velocity, U_s is the surface recombination rate, and Δn_s is the excess carrier density at the surface, S_{n0} and S_{p0} are the surface recombination velocities of electrons and holes, n_s and p_s are the electron and hole concentrations at the surface, σ_n and σ_p are the capture

cross-sections for electrons and holes, n_1 and p_1 are parameter in the SRH recombination equation and D_{it} is the number of surface states per unit area. However, if band bending exists on the Si surface by fixed charges (such as negative or positive charges), it is difficult to evaluate Δn_s because the carrier lifetime is determined by the carrier density in the bulk. To this end, we considered the surface of the semiconductor region ($z = 0$) and the space charge region ($z < d_{sc}$), as shown in Figure 5.

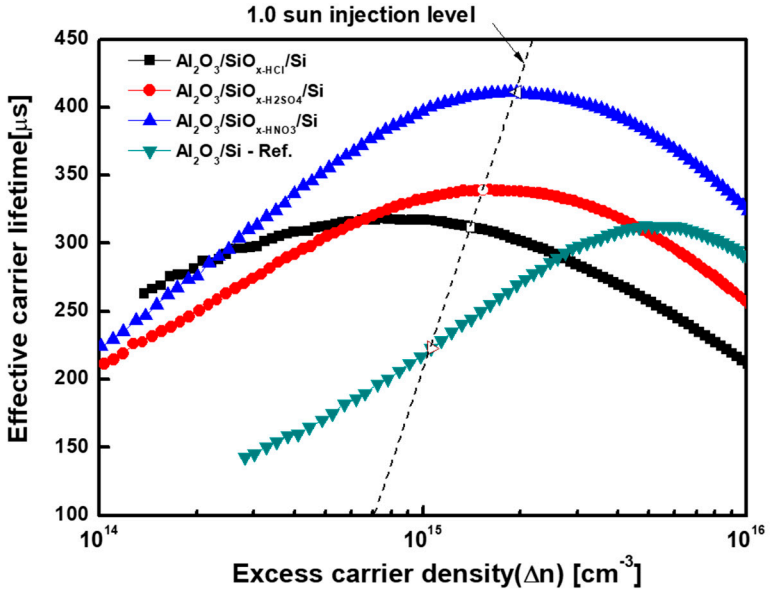

Figure 4. Effective carrier lifetime curves as a function of the excess carrier density (Δn) for $Al_2O_3/SiO_{x\text{-acidic}}$/Si structures and Al_2O_3/Si reference sample. The Al_2O_3 thickness is 10 nm and the SiO_x thicknesses are 1.49 nm for $SiO_{x\text{-HCl}}$, 1.32 nm for $SiO_{x\text{-H2SO4}}$, and 1.50 nm for $SiO_{x\text{-HNO3}}$, respectively.

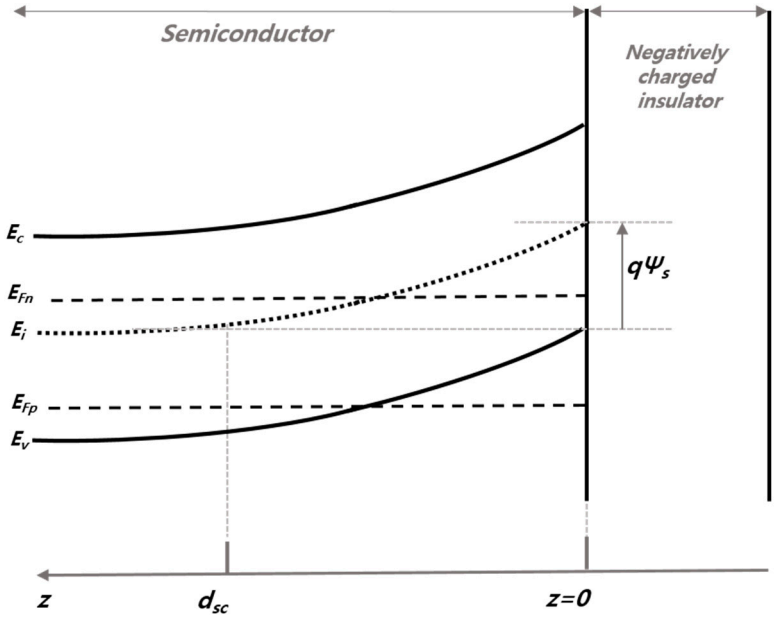

Figure 5. Energy band diagram for a semiconductor–insulator interface under illumination, where the semiconductor is p-type and the insulator is negatively charged (i.e., Al_2O_3). The diagram shows the energy of the conduction band E_c, the valence band E_v, the intrinsic fermi level E_i, as well as the quasi-fermi energy of electrons E_{Fn} and holes E_{Fp}. The distance $z = 0$ represents the interface between the semiconductor and the negatively charged insulator, and $z = d_{sc}$ represents the distance of the space charge region. Ψ_s is the surface potential.

Therefore, the effective surface recombination velocity (S_{eff}) is the sum of the interface recombination velocity and the space charge recombination velocity, as shown in Equations (3)–(9) [35–39].

$$S_{eff} = \frac{1}{\Delta n_{d_{sc}}}\left[U_s + \int_0^{d_{sc}} U(z)dz\right] = S_{it} + S_{sc} \tag{3}$$

S_{it} can be expressed in Equation (4) based on Equations (1) and (2).

$$S_{it} = \frac{1}{\Delta n_{d_{sc}}}\left[\frac{(n_s p_s - n_i^2)D_{it}V_{th}E_g}{\frac{n_s+n_1+\Delta n_s}{\sigma_p} + \frac{p_s+p_1+\Delta n_s}{\sigma_n}}\right] \tag{4}$$

S_{sc} can be described by Equation (5) as follows by using Equations (6)–(9) for surface potential (Ψ_s) and surface electron and hole concentrations by effective charge density (Q_f) [34,35].

$$S_{sc} = \frac{1}{\Delta n_{d_{sc}}}\int_0^{d_{sc}} \frac{(n_s(z)p_s(z) - n_i^2)N_{st}V_{th}E_g}{\frac{n_s(z)+n_1+\Delta n_{sc}}{\sigma_p} + \frac{p_s(z)+p_1+\Delta n_{sc}}{\sigma_n}}dz \tag{5}$$

$$\int_0^{d_{sc}} n_s(z)dz = \beta\lambda_D\int_{\Psi_s}^0 \frac{n(\Psi)}{F}d\Psi\,,\ \int_0^{d_{sc}} p_s(z)dz = \beta\lambda_D\int_{\Psi_s}^0 \frac{p(\Psi)}{F}d\Psi \tag{6}$$

$$Q_f = \mp\,\varepsilon_s\frac{F\left(\Psi_s, \Phi_p, \Phi_n\right)}{q\beta\lambda_D} \tag{7}$$

$$F\left(\Psi_s, \Phi_p, \Phi_n\right) = \sqrt{\frac{2}{p_b + n_b}\left[p_b\left(e^{-\beta\Psi_s} + \beta\Psi_s - 1\right) + n_b\left(e^{\beta\Psi_s} - \beta\Psi_s - 1\right)\right]} \tag{8}$$

$$p_b = n_i e^{\beta\Phi_p}\,,\ n_b = n_i e^{\beta\Phi_n} \tag{9}$$

Here, S_{it} is the interface recombination velocity between the Si surface and the dielectric layer ($z = 0$), S_{sc} is the recombination velocity in the space charge region ($z < d_{sc}$), d_{sc} is the distance of the space charge region, and z is the coordinate perpendicular to the semiconductor surface and increases toward the bulk of Si, V_{th} is the thermal carrier velocity, Eg is the energy band gap of Si, Ψ is the surface potential, Q_f is the fixed charge density, Φ_n and Φ_p are quasi-fermi level for electrons and holes, p_b and n_b are the carrier concentration for electrons and holes, n_i is intrinsic carrier concentration. With Equation (3), we can calculate the theoretical effective surface carrier lifetime using Equation (10).

$$\frac{1}{\tau_{eff}} = \frac{1}{\tau_{it}} + \frac{1}{\tau_{sc}} = \frac{W}{2}\left(\frac{1}{s_{it}} + \frac{1}{s_{sc}}\right) \tag{10}$$

where τ_{eff} is the effective surface carrier lifetime, τ_{it} is the carrier lifetime in the interface region between the Si surface and the dielectric layer, τ_{sc} is the carrier lifetime in the space charge region, and W is the thickness of the wafer. The surface carrier lifetime simulation was performed by comparing the effective carrier lifetime (τ_{measured}) measured using Equation (10). Assuming that the capture cross-section of the electron and hole is $\sigma_n = \sigma_p = 1 \times 10^{15}$ cm^2, we analyzed the interface trap density (D_{it}) and the fixed charge density (Q_f) as variable parameters so that the curves of $\tau_{\text{simulated}}$ and τ_{measured} matched well. Figure 6 shows the $\tau_{\text{simulated}}$ and τ_{measured} curves.

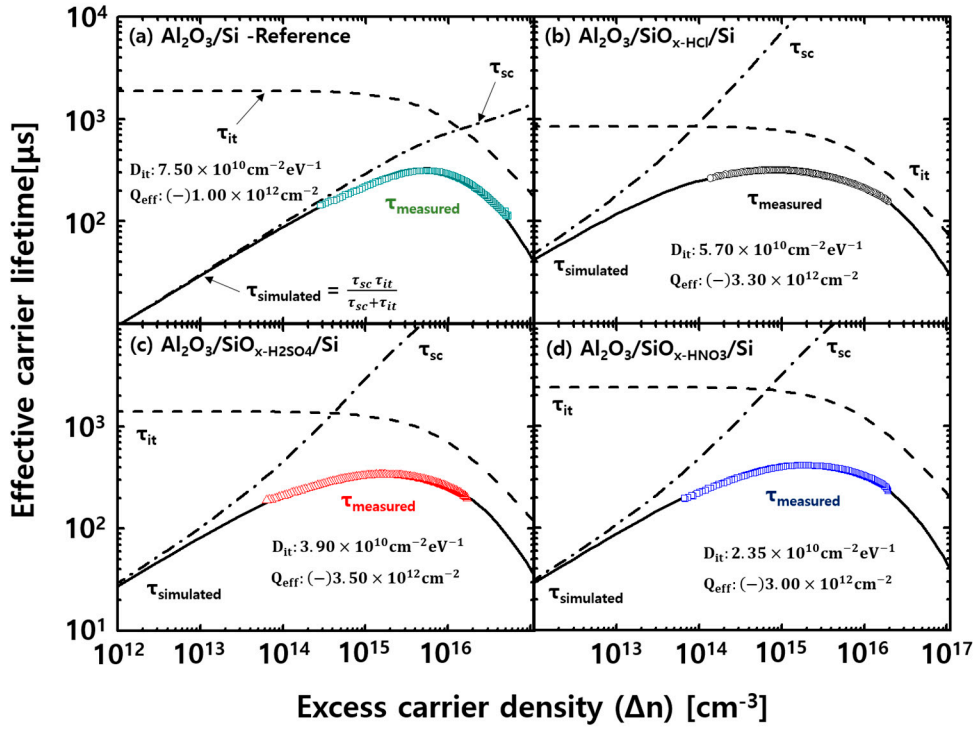

Figure 6. Measured and simulated effective carrier lifetime curves at $Al_2O_3/SiO_{x\text{-acidic}}$/Si structures as a function of excess carrier density (Δn). The solid line indicates the simulated effective carrier lifetime ($\tau_{simulated}$), the dash line indicates the effective carrier lifetime via interface state (τ_{it}), and the dotted dash line indicates the effective carrier lifetime via surface space charge region (τ_{sc}). The electron and hole capture cross-sections are assumed to be equal, $\sigma_n = \sigma_p = 1 \times 10^{15}$ cm^2.

The surface carrier lifetime analysis results show that the $Al_2O_3/SiO_{x\text{-HNO3}}/SiO_x$ sample exhibits a lower D_{it} (2.35×10^{10} cm^{-2}eV^{-1}) than the other samples (Table 2). The effective charge densities are similar regardless of the acidic solution used. Considering the lifetime of the $SiO_{x\text{-HNO3}}$ layer and values of Q_f and D_{it} extracted from the surface carrier lifetime analysis, the passivation properties would be more influenced by D_{it} than Q_f. C–V measurements were also performed to compare the values of D_{it} and Q_f with those obtained from the surface carrier lifetime analysis. The C–V measurement results show that V_{FB} (flat band voltage) of the silicon substrates with wet chemical oxide layers shifts by 1.77–2.08 V toward the positive bias, as shown in Figure 7.

Table 2. Results of capacitance–voltage (C–V) and surface carrier lifetime analyses.

Sample (Average of Five Samples)	Capacitance–Voltage (C–V) Analysis			Surface Carrier Lifetime Analysis	
	Q_f (10^{12} cm^{-2})	D_{it} (10^{10} cm^{-2}eV^{-1})	V_{FB} (V)	Q_f (10^{12} cm^{-2})	D_{it} (10^{10} cm^{-2}eV^{-1})
Al_2O_3/Si	−1.53	7.01	1.20	−1.00	7.50
$Al_2O_3/SiO_{x\text{-HCl}}$/Si	−3.03	4.94	2.97	−3.30	5.70
$Al_2O_3/SiO_{x\text{-H2SO4}}$/Si	−3.12	4.60	3.12	−3.50	3.90
$Al_2O_3/SiO_{x\text{-HNO3}}$/Si	−3.24	2.88	3.28	−3.52	2.30

Q_f was calculated using V_{FB} extracted from the measured C–V graph, and D_{it} was obtained using the Terman method (Table 2) [40,41]. The negative Q_f values of the silicon oxides formed in the different acidic solutions did not change significantly in the range of 3.03–3.24 $\times 10^{12}$ cm^{-2}. However, D_{it} was markedly different depending on the acid solution used (Table 2). Therefore, we confirm that the quality of SiO_x at the Al_2O_3/Si interface affects the passivation characteristics, and the insertion of a wet

chemical oxide layer improved the passivation quality, compared with the SiO_x layer simultaneously formed during the deposition of Al_2O_3.

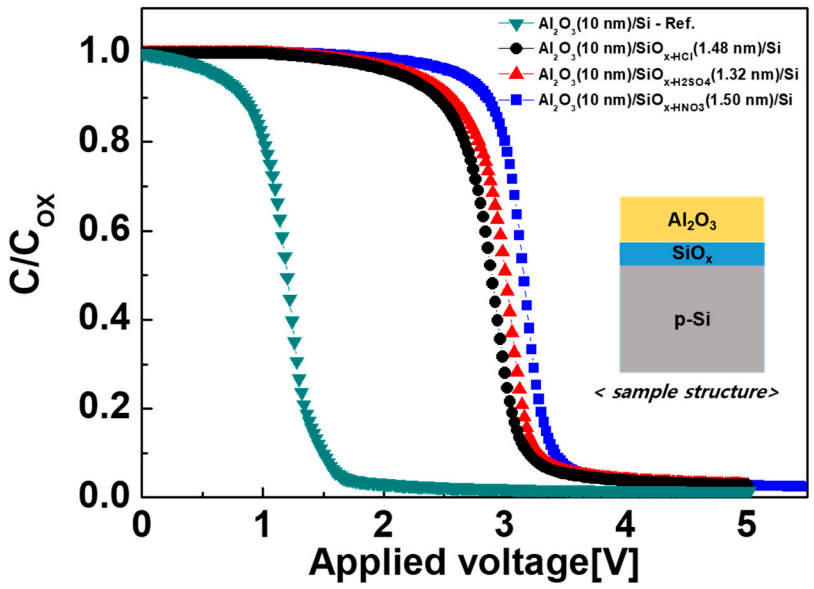

Figure 7. Capacitance–voltage curves at 1 MHz of $Al_2O_3/SiO_{x\text{-acidic}}$/Si structures and Al_2O_3/Si reference sample for calculating the fixed charge density (Q_f) and interface trap density (D_{it}).

4. Conclusions

In this study, we improved the interfacial properties of an Al_2O_3/Si structure by performing wet chemical oxidation on an Si substrate. The thickness of the wet chemical oxides grown on the Si surface in different acidic solutions was in the range of 1.32–1.5 nm, which was similar to that of SiO_x naturally formed at the interface of the Al_2O_3/Si sample during PA-ALD deposition. In particular, $SiO_{x\text{-}HNO3}$ showed a relatively lower leakage current than $SiO_{x\text{-}HCl}$ and $SiO_{x\text{-}H2SO4}$. The carrier lifetime of $Al_2O_3/SiO_{x\text{-}HNO3}$/Si measured by QSSPC to evaluate the passivation characteristics was ~ 400 µs, which was higher than those of the other $SiO_{x\text{-acidic}}$ layers (~317 µs for $SiO_{x\text{-}HCl}$ and ~332 µs for $SiO_{x\text{-}H2SO4}$). C–V measurement and surface carrier lifetime analysis were performed to analyze the interface characteristics of the Al_2O_3/SiO_x/Si samples. The fixed charges showed little change with the oxides, and the D_{it} values changed significantly. The wet chemical oxide formed in the HNO_3 solution showed better passivation characteristics than those formed in other acidic solutions, resulting from the low interface trap density of $SiO_{x\text{-}HNO3}$. We confirmed the improvement in the passivation characteristics of the Al_2O_3/Si sample by inserting a wet chemical oxide between Al_2O_3 and Si substrates. In addition, the values of the parameters associated with the interface properties, such as Q_f and D_{it}, obtained from the C–V measurement and surface carrier lifetime simulation were similar. Therefore, this simulation can be a useful tool to analyze interfacial characteristics. Moreover, this study lays a foundation for analyzing the interfacial properties of samples, such as poly-Si/SiO_x/Si structures with ultra-thin SiO_x, that cannot be analyzed by C–V measurements.

Author Contributions: K.H.M. designed experiments, performed the experiments and wrote manuscripts; H.-e.S. and H.-S.L. wrote manuscripts and interpreted experimental findings; S.P., M.G.K., J.I.L., Y.K., D.K. supervised the studies; S.C. and M.S.J. participated in discussion. All authors have read and agreed to the published version of the manuscript.

Funding: This work was conducted under the framework of the Research and Development of the Korea Institute of Energy Research (C0-2402); the Technology Development Program to Solve Climate Changes of the National Research Foundation (NRF) funded by the Ministry of Science, ICT and Future Planning (2017M1A2A2086911).

Conflicts of Interest: The authors declare no conflict of interest.

References

1. King, R.R.; Sinton, R.A. Studies of diffused phosphorus emitters: Saturation current, surface recombination velocity, and quantum efficiency. *IEEE Trans. Electron. Dev.* **1990**, *37*, 365–371. [CrossRef]
2. Cuevas, A.; Basore, P.A.; Giroult-Matlakowski, G.; Dubois, C. Surface recombination velocity of highly doped n-type silicon. *J. Appl. Phys.* **1996**, *80*, 3370–3375. [CrossRef]
3. Blakers, A.W.; Wang, A.; Milne, A.M.; Zhao, J.; Green, M.A. 22.8% efficient silicon solar cell. *Appl. Phys. Lett.* **1989**, *55*, 1363–1365. [CrossRef]
4. Sterk, S.; Glunz, S.W.; Knobloch, J.; Wettling, W. High efficiency (>22%) Si-solar cells with optimized emitter. In Proceedings of the IEEE 1st World Conference on Photovoltaic Energy Conversion, Waikoloa, HI, USA, 5–9 December 1994.
5. Zhang, S.; Yao, Y.; Hu, D.; Lian, W.; Qian, H.; Jie, J.; Wei, Q.; Ni, Z.; Zhang, X.; Xie, L. Application of silicon oxide on high efficiency monocrystalline silicon PERC solar cells. *Energies* **2019**, *12*, 1168. [CrossRef]
6. Gong, L.; Zhou, C.; Zhu, J.; Wang, W. Passivation characteristics of new silicon oxide. *IEEE J. Photovolt.* **2019**, *9*, 1873–1879. [CrossRef]
7. Aberle, A.G.; Lauinger, T.; Schmidt, J.; Hezel, R. Injection-level dependent surface recombination velocities at the silicon-plasma silicon nitride interface. *Appl. Phys. Lett.* **1995**, *66*, 2828–2830. [CrossRef]
8. Schmidt, J.; Aberle, A.G. Carrier recombination at silicon–silicon nitride interfaces fabricated by plasma-enhanced chemical vapor deposition. *J. Appl. Phys.* **1999**, *85*, 3626–3633. [CrossRef]
9. Lelièvre, J.-F.; Kafle, B.; Saint-Cast, P.; Brunet, P.; Magnan, R.; Hernandez, E.; Pouliquen, S.; Massines, F. Efficient silicon nitride SiN_x:H antireflective and passivation layers deposited by atmospheric pressure PECVD for silicon solar cells. *Prog. Photovolt. Res. Appl.* **2020**, *27*, 1007–1019. [CrossRef]
10. Hoex, B.; Schmidt, J.; Bock, R.; Altermatt, P.P.; Van de Sanden, M.C.M.; Kessels, W.M.M. Excellent passivation of highly doped p-type Si surfaces by the negative-charge-dielectric Al_2O_3. *Appl. Phys. Lett.* **2007**, *91*, 112107. [CrossRef]
11. Richter, A.; Benick, J.; Hermle, M. Boron emitter passivation with Al_2O_3 and Al_2O_3/SiN_x stacks using ALD Al_2O. *IEEE J. Photovolt.* **2013**, *3*, 236–245. [CrossRef]
12. Lin, Y.-H.; Wu, Y.-C.; You, H.-C.; Chen, C.-H.; Chen, P.-H.; Tsai, Y.-H.; Yang, Y.-Y.; Chang-Liao, K.S. Silicon heterojunction solar cells using AlO_x and plasma-immersion ion implantation. *Energies* **2014**, *7*, 3653–3663. [CrossRef]
13. Dicks, O.A.; Cottom, J.; Shluger, A.L.; Afamas'ev, V.V. The origin of negative charging in amorphous Al_2O_3 films: The role of native defects. *Nanotechnology* **2019**, *30*, 205201. [CrossRef] [PubMed]
14. Yang, X.; Weber, K.; Hameiri, Z.; De Wolf, S. Industrially feasible, dopant-free, carrier-selective contacts for high-efficiency silicon solar cells. *Prog. Photovolt. Res. Appl.* **2017**, *25*, 896–904. [CrossRef]
15. Lee, Y.-T.; Lin, F.-R.; Lin, T.-C.; Chen, C.-H.; Pei, Z. Low-temperature, chemically grown titanium oxide thin films with a high hole tunneling rate for Si solar cells. *Energies* **2016**, *9*, 402. [CrossRef]
16. Chen, T.-C.; Yang, T.-C.; Cheng, H.-E.; Yu, I.-S.; Yang, Z.-P. Single material TiO_2 thin film by atomic layer deposition for antireflection and surface passivation applications on p-type c-Si. *Appl. Surf. Sci.* **2018**, *451*, 121–127. [CrossRef]
17. Geissbühler, J.; Werner, J.; Martin de Nicolas, S.; Barraud, L.; Hessler-Wyser, A.; Despeisse, M.; Nicolay, S.; Tomasi, A.; Niesen, B.; De Wolf, S.; et al. 22.5% efficient silicon heterojunction solar cell with molybdenum oxide hole collector. *Appl. Phys. Lett.* **2015**, *107*, 081601. [CrossRef]
18. Bivour, M.; Temmler, J.; Steinkemper, H.; Hermle, M. Molybdenum and tungsten oxide: High work function wide band gap contact materials for hole selective contacts of silicon solar cells. *Sol. Energy. Mater. Sol. Cells* **2015**, *142*, 34–41. [CrossRef]
19. Römer, U.; Peibst, R.; Ohrdes, T.; Lim, B.; Krügener, J.; Wietler, T.; Brendel, R. Ion implantation for poly-Si passivated back-junction back-contacted solar cells. *IEEE J. Photovolt.* **2015**, *5*, 507–514. [CrossRef]
20. Moldovan, A.; Feldmann, F.; Zimmer, M.; Rentsch, J.; Benick, J.; Hermle, M. Tunnel oxide passivated carrier-selective contacts based on ultra-thin SiO_2 layers. *Sol. Energy Mater. Sol. Cells* **2015**, *142*, 123–127. [CrossRef]
21. Choi, S.; Min, K.H.; Jeon, M.S.; Lee, J.I.; Kang, M.G.; Song, H.-E.; Kang, Y.; Lee, H.-S.; Kim, D.; Kim, K.-H. Structural evolution of tunneling oxide passivating contact upon thermal annealing. *Sci. Rep.* **2017**, *7*, 12853. [CrossRef]

22. Feldmann, F.; Reichel, C.; Müller, R.; Hermle, M. The application of poly-Si/SiOx contacts as passivated top/rear contacts in Si solar cells. *Sol. Energy. Mater. Sol. Cells* **2017**, *159*, 256–271. [CrossRef]
23. Hoex, B.; Gielis, J.J.H.; van de Sanden, M.C.M.; Kessels, W.M.M. On the *c*-Si surface passivation mechanism by the negative-charge-dielectric Al_2O_3. *J. Appl. Phys.* **2008**, *104*, 1113703. [CrossRef]
24. Naumann, V.; Otto, M.; Wehrspohn, R.B.; Werner, M.; Hagendorf, C. Interface and material characterization of thin ALD-Al_2O_3 layers on crystalline silicon. *Energy Procedia* **2012**, *27*, 312–318. [CrossRef]
25. Kersten, F.; Schmid, A.; Bordihn, S.; Müller, J.W.; Heitmann, J. Role of annealing conditions on surface passivation properties of ALD Al_2O_3 films. *Energy Procedia* **2013**, *38*, 843–848. [CrossRef]
26. Veith, B.; Werner, F.; Zielke, D.; Brendel, R.; Schmidt, J. Comparison of the thermal stability of single Al_2O_3 layers and Al_2O_3/SiN_x stacks for the surface passivation of silicon. *Energy Procedia* **2011**, *8*, 307–312. [CrossRef]
27. Dingemans, G.; Terlinden, N.M.; Verheijen, M.A.; van de Sanden, M.C.M.; Kessels, W.M.M. Controlling the fixed charge and passivation properties of Si(100)/Al_2O_3 interfaces using ultrathin SiO_2 interlayers synthesized by atomic layer deposition. *J. Appl. Phys.* **2011**, *110*, 093715. [CrossRef]
28. Kobayashi, H.; Yamashita, Y.; Nakato, Y.; Komeda, T.; Nishioka, Y. Interface states at ultrathin oxide/Si(111) interfaces obtained from x-ray photoelectron spectroscopy measurements under biases. *Appl. Phys. Lett.* **1996**, *69*, 2276–2278. [CrossRef]
29. Imamura, K.; Takahashi, M.; Asuha; Hirayama, Y.; Imai, S.; Kobayashi, H. Nitric acid oxidation of Si method at 120 °C: HNO_3 concentration dependence. *J. Appl. Phys.* **2010**, *107*, 054503. [CrossRef]
30. Kobayashi Asuha, H.; Maida, O.; Takahashi, M.; Iwasa, H. Nitric acid oxidation of Si to form ultrathin silicon dioxide layers with a low leakage current density. *J. Appl. Phys.* **2003**, *94*, 7328–7335. [CrossRef]
31. Laades, A.; Angermann, H.; Sperlich, H.-P.; Stürzebecher, U.; Álvarez, C.A.D.; Bähr, M.; Lawerenz, A. Wet chemical oxidation of silicon surfaces prior to the deposition of all-PECVD AlO_x/a-SiN_x passivation stacks for silicon solar cells. *Solid State Phenom.* **2013**, *195*, 310–313. [CrossRef]
32. Bordihn, S.; Engelhart, P.; Mertens, V.; Kesser, G.; Köhn, D.; Dingemans, G.; Mandoc, M.M.; Müller, J.W.; Kessels, W.M.M. High surface passivation quality and thermal stability of ALD Al_2O_3 on wet chemical grown ultra-thin SiO_2 on silicon. *Energy Procedia* **2011**, *8*, 654–659. [CrossRef]
33. Kern, W. The evolution of silicon wafer cleaning technology. *J. Elecrochem. Soc.* **1990**, *137*, 1887–1892. [CrossRef]
34. Sinton, R.A.; Cuevas, A. Contactless determination of current-voltage characteristics and minority carrier lifetimes in semiconductors from quasi-steady-state photoconductance data. *Appl. Phys. Lett.* **1996**, *69*, 2510–2512. [CrossRef]
35. Aberle, A.G. *Crystalline Silicon Solar Cells, Advanced Surface Passivation and Analysis*; UNSW: Sydney, Australia, 2009.
36. Bonilla, R.S.; Hoex, B.; Hamer, P.; Wilshaw, P.R. Dielectric surface passivation for silicon solar cells: A review. *Phys. Status Solidi A* **2017**, *214*, 1700293. [CrossRef]
37. Schmidt, J.; Moschner, J.D.; Henze, J.; Dauwe, S.; Hezel, R. Recent progress in the surface passivation of silicon solar cells using silicon nitride. In Proceedings of the 19th European Photovoltaic Solar Energy Conference, Paris, France, 7–11 June 2004; pp. 391–396.
38. McIntosh, K.R.; Black, L.E. On effective surface recombination parameters. *J. Appl. Phys.* **2014**, *116*, 014503. [CrossRef]
39. Ma, F.-J.; Hoex, B.; Samudra, G.S.; Aberle, A.G. Modelling and simulation of field-effect surface passivation of crystalline silicon-based solar cells. *Energy Procedia* **2012**, *15*, 155–161. [CrossRef]
40. Terman, L.M. An investigation of surface states at a silicon/silicon oxide interface employing metal-oxide-silicon diodes. *Solid State Electron.* **1962**, *5*, 285–299. [CrossRef]
41. Nicollian, E.H.; Brews, J.R. *MOS (Metal Oxide Semiconductor) Physics and Technology*; Wiley: New York, NY, USA, 1982.